PROCEEDINGS OF SPIE

SPIEDigitalLibrary.org/conference-proceedings-of-spie

3D tomography of shark vertebrae via energy dispersive diffraction

Stock, S., Morse, P., Stock, M., James, K., Natanson, L., et al.

S. R. Stock, P. E. Morse, M. K. Stock, K. C. James, L. J. Natanson, H. Chen, P. V. Shevchenko, E. R. Maxey, O. Antipova, J. S. Park, "3D tomography of shark vertebrae via energy dispersive diffraction," Proc. SPIE 11840, Developments in X-Ray Tomography XIII, 118400N (9 September 2021); doi: 10.1117/12.2595040

SPIE.

Event: SPIE Optical Engineering + Applications, 2021, San Diego, California, United States

Microstructure and energy dispersive diffraction reconstruction of 3D patterns of crystallographic texture in a shark centrum

S.R. Stock,[a,*] P.E. Morse[b,c], M.K. Stock[d], K.C. James[e], L.J. Natanson[f], Haiyan Chen[g], P.D. Shevchenko[h], E.R. Maxey[h], O. Antipova[h], J.-S. Park[h]

[a] Dept. of Cell and Developmental Biology, Feinberg School of Medicine, and Simpson Querrey Inst., Northwestern Univ., Chicago, IL, USA

[b] Dept. of Evolutionary Anthropology, Duke Univ., Durham, NC, USA

[c] Florida Museum of Natural History, Univ. of Florida, Gainesville, FL, USA

[d] Dept. of Sociology & Anthropology, Metropolitan State Univ. of Denver, Denver, CO, USA

[e] Southwest Fisheries Science Center, National Marine Fisheries Service, NOAA, La Jolla, CA USA

[f] (retired) Northeast Fisheries Science Center, National Marine Fisheries Service, NOAA, Narragansett, RI, USA

[g] Mineral Physics Inst., Stony Brook Univ., Stony Brook, NY, USA

[h] Advanced Photon Source, Argonne National Laboratory, Lemont, IL, USA

ABSTRACT

Tomography using diffracted x-rays produces reconstructions mapping quantities including crystal lattice parameter(s), crystallite size and crystallographic texture; this information is quite different from that obtained with absorption contrast or phase contrast. Diffraction tomography can be performed using energy dispersive diffraction (EDD) and polychromatic synchrotron x-radiation. In EDD, different, properly-oriented Bragg planes diffract different x-ray energies; these intensities are measured by an energy sensitive detector. A pencil beam defines the irradiated volume, and a collimator before the energy sensitive detector selects which portion of the irradiated column is sampled at any one time. A 3D map is assembled by translating the specimen along X, Y and Z axes. This paper reports results of 3D mapping of the integrated intensity of several reflections from the bioapatite in the mineralized cartilage centrum of a blue shark. The multiple detector EDD system at 6-BM-B, the Advanced Photon Source was used to map an entire blue shark centrum. The shark centrum consists of a double cone structure (corpora calcerea) supported by the intermedialia consisting of four wedges. The integrated intensities of the *c*-axis reflection and of a reflection with no c-axis component reveals the bioapatite within the cone wall is oriented with its *c*-axes lateral, i.e., perpendicular to the axis of the backbone, whereas the bioapatite within the wedges is oriented with its *c*-axes axial. Results of absorption microCT (laboratory and synchrotron) and x-ray excited x-ray fluorescence mapping are included to provide higher resolution data of the structures underlying the EDD maps. Application of EDD tomography to 3D mapping of large specimens promises to add to the understanding of other mineralized tissue samples which cannot be sectioned.

Keywords: energy dispersive diffraction, microCT, x-ray fluorescence, shark, vertebra, mineralized cartilage, bioapatite

1. INTRODUCTION

Sharks have cartilaginous skeletons, and each vertebra of their vertebral column contains a mineralized centrum which carries the loads generated during swimming.[1] The structure and mineralization of the centra enables shark vertebrae to survive enormous compressive strains of 3-8%[2] for millions of cycles of loading[3], despite the absence of a repair mechanism analogous to remodeling in bone. Diffraction has shown that the centra's mineral is a bioapatite closely related to hydroxyapatite (hAp)[4,5] and that the bioapatite is organized similarly to bone[6].

Shark centra have complex 3D structures, and the focus in this paper is on the abdominal centra of the blue shark (*Prionace glauca*, Carcharhiniformes). Each centrum consists of an hourglass-shaped double cone, the corporus calcerea, of mineralized cartilage ("c" in Fig. 1). A fluid filled inter-vertebral capsule lies between the cone walls of adjacent vertebrae.

* s-stock@northwestern.edu

Developments in X-Ray Tomography XIII, edited by Bert Müller
Ge Wang, Proc. of SPIE Vol. 11840, 118400N · © 2021 SPIE
CCC code: 0277-786X/21/$21 · doi: 10.1117/12.2595040

Within a blue shark single centrum, the rostral and caudal cone walls are supported by the intermedialia consisting of four thick wedges ("W" in Fig. 1) with unmineralized gaps "g" separating the wedges. Centra macrostructure differs between carcharhiniform species.[7] During swimming, both the left and right sides of shark abdominal centra experience an alternating pattern of compression and tension (Fig. 1). Some studies of the macroscopic patterns of strain in the shark spine have appeared,[1,2,8] but little is known about the 3D distributions of displacement or of strain within the complex structure of a shark centrum or even the presence or absence of bioapatite crystallographic texture.

The study reported below uses a novel approach, energy dispersive diffraction (EDD) with polychromatic synchrotron x-radiation, to map in 3D the spatial organization of bioapatite and its crystallographic texture in a blue shark centrum. In particular, the authors ask whether weak diffraction peaks can still produce an informative reconstruction. Results from microComputed Tomography (microCT) and from scanning x-ray excited x-ray fluorescence are used to help interpret the EDD maps. The EDD results are then interpreted in light of what is known about patterns of in vivo loading. Finally, prospects for future EDD mapping of shark centra are discussed.

2. MATERIALS AND METHODS

One complete abdominal vertebra of a blue shark (*Prionace glauca*, Carcharhiniformes, from vertebrae numbers 81-84) was studied first with lab microCT and later with EDD mapping. The diameter and height of the vertebra's centrum were 24.3 mm and 12.7 mm, respectively. A second vertebrae from the shark was cut into sections parallel to the vertebral column's axis and less than 1 mm thick (Fig. 1) or into similarly oriented blocks with roughly square cross-sections ~2.5 mm across.
The former were used for fluorescence mapping, and the latter for synchrotron microCT.

The lab microCT scan of the frozen blue shark centrum was performed with the Nikon XTH 225 ST system at the Shared Materials Instrumentation Facility at Duke University. The centrum was placed approximately at the center of the scanner rotation axis. The x-ray tube was operated at 140 kVp and 111 μA with a 0.125 mm thick Cu filter. Four frames were averaged per projection with 500 ms integration per frame, and 2,500 projections were recorded over 360°. The volume was reconstructed with isotropic 18.4 μm volume elements (voxels).

X-ray excited x-ray fluorescence mapping provided maps of elemental composition of a section of a blue shark centrum and was performed at two beam lines at the Advanced Photon Source (APS). The section was parallel to the clipping plane of the left image of Fig. 1b. At beamline 8-BM-B, Kirkpatrick-Baez optics focused the beam of 15.3 keV x-rays to ~ 20 μm diameter.[9] The sample was rastered across the beam, and maps of the fluorescent intensity were recorded. At beamline

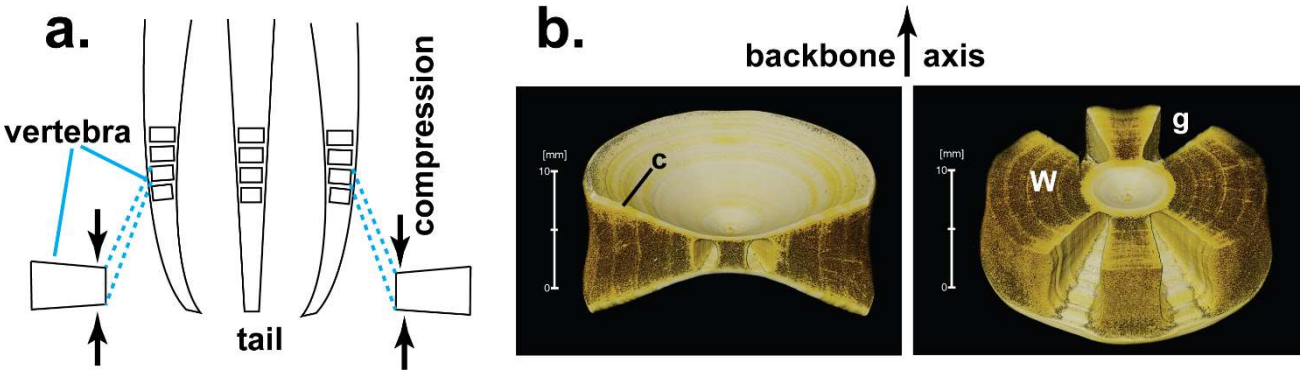

Fig. 1. (a) Vertebral compression when a shark swims, illustrated schematically by three positions of the tail. When the tail swings to the right (left tail diagram), the right side of the vertebra is compressed as indicated by the compression of the right side of the vertebra (left trapezoid with arrows indicating compression). As the right side of the schematic indicates, the vertebra's opposite (left) side compresses when the tail moves to the left. (b) Lab microCT-derived renderings of the blue shark centrum with the portions closest to the viewer rendered transparent (left - axial clipping plane and right - transverse clipping plane). The axial clipping plane shows the section orientation for x-ray fluorescence mapping (Fig. 4). c - hourglass-shaped cone of mineralized cartilage, W – wedges of the intermedialia, g – gaps separating the wedges.

2-ID-E, APS, Fresnel optics produced a 0.4-0.45 μm diameter beam of 13.7 keV photons. A small portion of the same section was scanned at much higher resolution than at 8-BM. The 2-ID-E apparatus is described elsewhere.[10]

Synchrotron microCT was performed at beamline 2-BM, APS. A block of a blue shark centrum was imaged with 24.35 keV x-ray photons and 1500 projections over 180°. The 2448 x 2448 voxel slices were reconstructed with 0.69 μm voxels.

Energy dispersive x-ray diffraction mapping of a blue shark centrum in 50% ethanol was performed at beamline 6-BM-B, APS, and employed a unique array of ten energy sensitive detectors.[11] Figure 2 is a schematic of instrument and the three orthogonal axes X (horizontal, perpendicular to the incident beam), Y (vertical, normal to the incident beam) and Z (horizontal, parallel to the incident beam). A collimator forms a pencil beam of polychromatic radiation (dimensions δX x δY of 0.1 x 0.2 mm) which passes through the specimen (here a transverse section near the middle of a blue shark centrum). Conical receiving slits "cs" block all radiation except that diffracted from the sampling volume "sv" at an angle $2\theta = 6.5°$. The incident beam gage length was $\delta Z = 1.7$ mm, as determined by translating a ~0.9 mm thick powdered ceria standard (NIST SRM 674B) across the sampling volume and by measuring the full-width at half-maximum of diffracted peak intensities. The centrum was scanned across the sampling volume using translation increments of $\Delta X = 2.0$ mm, $\Delta Y = 1.0$ mm and $\Delta Z = 1.9$ mm and 30 s/position exposures. The integrated intensity for each reflection was determined by fitting with a pseudoVoigt function.[6,12] The 3D volume was reconstructed on a 0.5 mm x 0.5 mm x 0.5 mm grid with interpolation of the neighboring voxels and smoothing. The ten energy sensitive detectors (Fig. 2b) simultaneously collect diffracted intensity from crystallites with different orientations.

Shark centra contain a myriad of nanoparticles of bioapatite,[6] and some of them are oriented to diffract one periodicity (d-spacing d_A) selecting x-ray photons with energy E_A and others another periodicity d_B with energy E_B. Each detector records intensity as a function of x-ray energy, and different periodicities produce diffraction peaks at different energies. From the known energy (and its inverse, x-ray wavelength λ), Bragg's law, $\lambda = 2\ d \sin\theta$ allows values of d to be determined for each peak, given the diffraction angle is $2\theta = 6.5°$. The analysis presented below focuses on the integrated intensity of the 00.2 peak, the 13.0 peak and unresolved 21.1, 11.2, 30.0 and 20.2 quadruplet of peaks hereafter designated peak "q". †

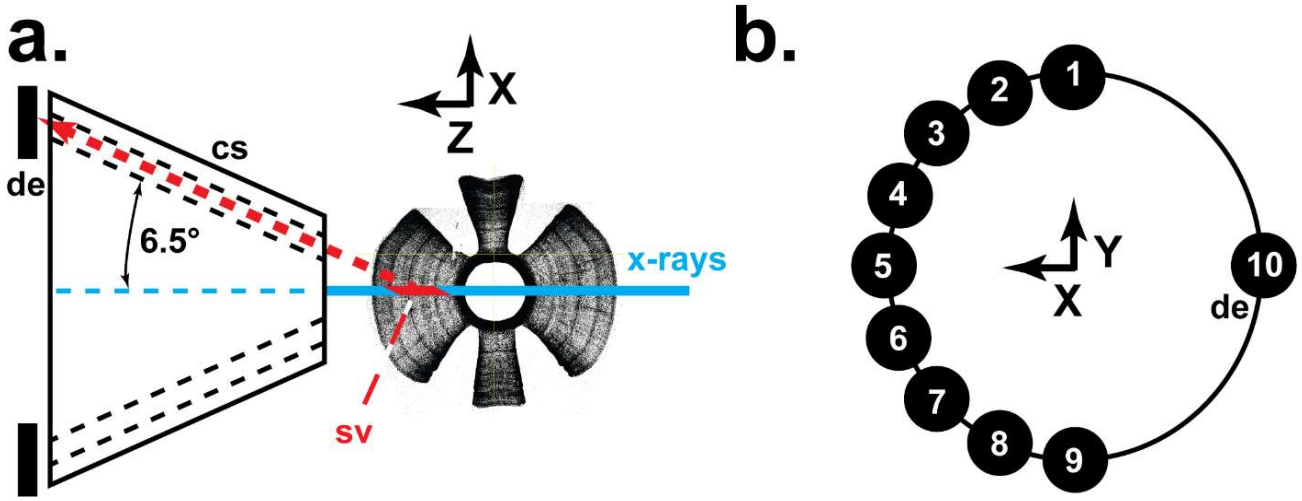

Fig. 2. (a) Schematic of the EDD with a transverse section of the blue shark centrum. sv – sampling volume, cs – conical receiving slits, de – detector elements. (b) Detector array with detector 1-10 indicated.

† Here the abbreviated Miller-Bravais indexing system is used to emphasize the hexagonal crystal system of the bioapatite.[13]

3. RESULTS AND DISCUSSION

Figure 3 shows lab microCT images of an entire blue shark centrum. The three orthogonal sections reveal the geometry of the cone “c” (corporus calcerea), wedge “W” (intermedialia) and gap “g” (between mineralized wedges). The cone appears to average higher mineral density than the wedges. In the transverse section, narrow high attenuation features run circumferentially within the wedges; these are growth bands and one is labeled “gb”. Numerous other circumferential structures appear between the periodic high attenuation bands. The growth bands are also visible in the two axial sections. Cartilage canals can barely be seen running radially within the wedges. The area with the box is enlarged in the inset (lower right in Fig. 3) and focuses on a single cartilage canal “cc” which is on the order of 2 voxels wide (35-40 µm) and which has a border of higher attenuation voxels which one would interpret as a thin hypermineralized zone. Elsewhere ~90 µm diameter cartilage canals were seen. The cone wall’s external borders and the surfaces of the wedges with the gaps also appear to be hypermineralized.

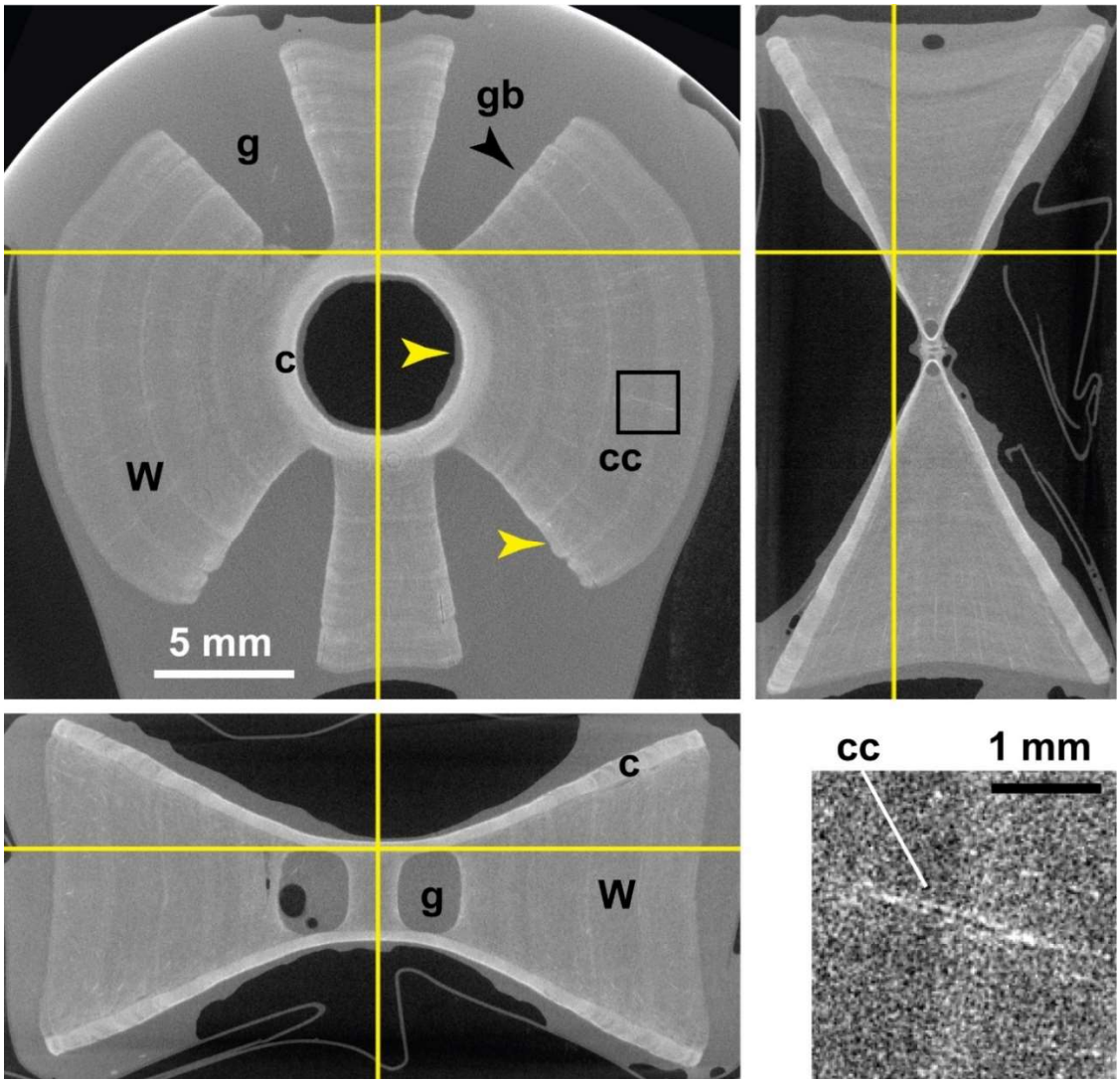

Fig. 3. Three orthogonal sections through the lab microCT data set for the blue shark centrum. The yellow lines indicate the positions of the sections, and the boxed area labeled “cc” is enlarged in the inset panel at the lower right. Here and in Fig. 5 and 6, the lighter the pixel, the higher the linear attenuation coefficient of the voxel. The horizontal arrowheads point to regions of higher mineral level. The following structures are labeled: W – wedge; c – cone; g – gap between wedges; gb – growth bands; cc – cartilage canal.

Figure 4 shows P, Ca and Zn scanning fluorescence maps (blue, red and green, respectively) of a blue shark centrum section in the orientation indicated in Fig. 1, i.e., at about the same position as the bottom left panel of Fig. 3. The apparent distortion top to bottom of these images is due to the section being slightly oblique relative to the centrum axis. The magenta contrast in the composite (Ca+Zn+P) maps shows where Ca and P but not Zn are concentrated, and white contrast indicates high intensities of all three. The cones have higher Ca and P intensities than the wedge tissue, and this demonstrates the cones' mineral density is higher than that of the intermedialia. Bands of strong vs low Ca and P intensity indicate modulated bioapatite content, and the complex band structure seen in lab microCT is also clear in the Ca and P fluorescence maps. The growth band substructure appears less distinct in the Zn maps, however, perhaps because the Zn photons emerge from much greater depths than the Ca or P signals and slight tilts would obscure narrow features. Such bands were observed previously in x-ray fluorescence maps.[14] At the right (lateral) side of centrum map in Fig. 4a, there are a closely spaced series of high intensity Ca and P bands, bands which were not seen in the centrum of Fig. 3. The outermost band in the composite (Ca+Zn+P) map of Fig. 4a is white, indicating that all three elements are concentrated in the lateral outer surface of the intermedialia. A green band is present outside the white band, a characteristic of ongoing biomineralization.[15] This enhanced Zn content is, however, non-specific because there are many matrix metalloproteinases and other Zn containing macromolecules involved in biomineralization. Histology with labels for specific macromolecules

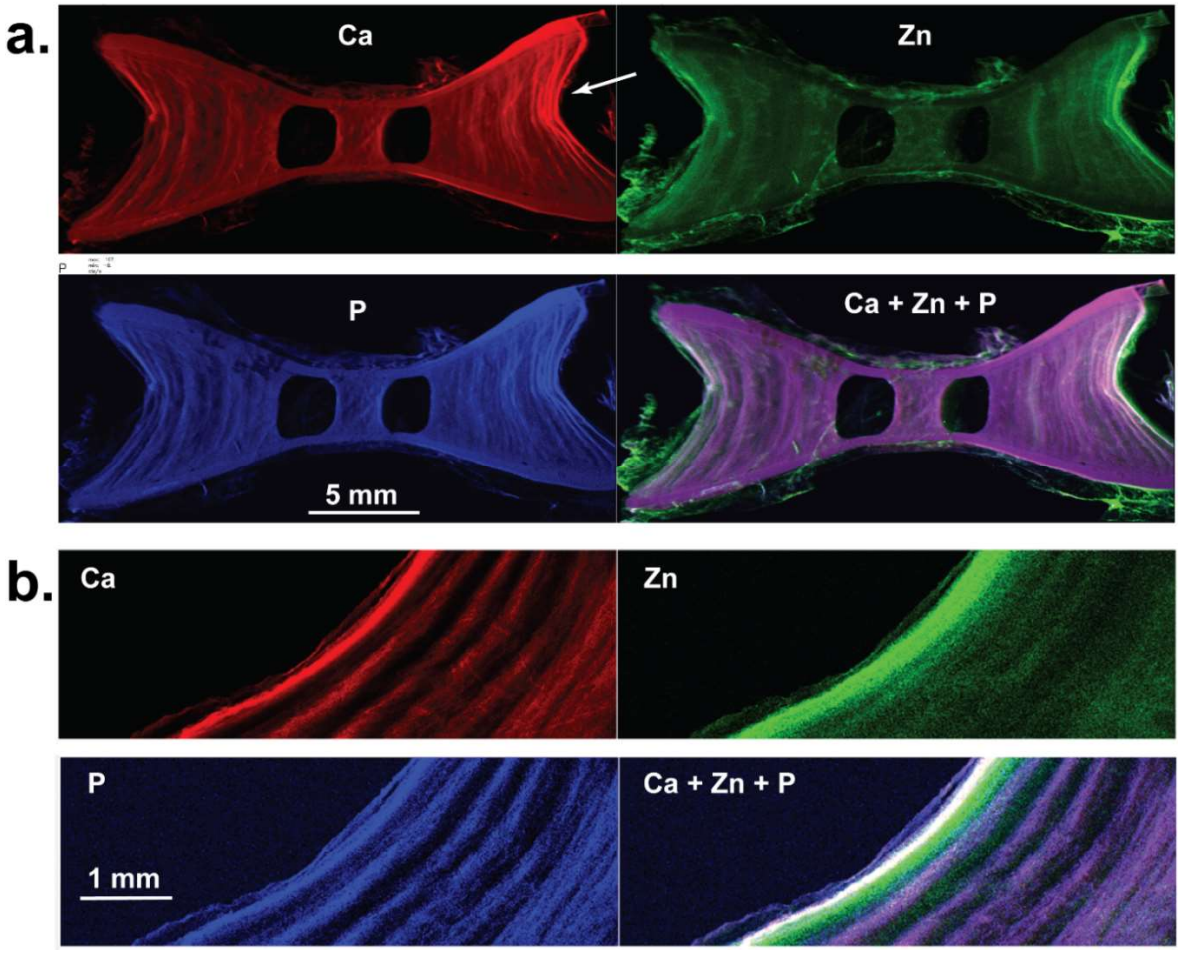

Fig. 4. X-ray excited scanning fluorescence map of Ca, Zn and P intensities along with a composite Ca+Zn+P of the three intensities. The brighter the color, the greater the intensity. (a) Map recorded at 8-BM and covering the entire section. The Ca, Zn and P maximum intensities were 7,063; 176 and 167 cts/s, respectively. The white arrow in the Ca panel indicates the approximate position mapped at 2-ID-E. (b) Map recorded of a portion of the same section at 2-ID-E. The section was oriented slightly differently than in the 8-BM data, and the horizontal axis of the maps are reflected relative to the first panels. The Ca, Zn and P maximum intensities were 87,324, 2,223 and 1,516 cts, respectively.

would be required to identify the macromolecules present; however, having a specific indication of where to look is very important. The maps of Fig. 4b are tilted relative to those in Fig. 4a and are reflected from left to right. In Fig. 4b, the five closely and evenly spaced Ca+P bands are present at the outer surface of the wedge. In contrast with Fig. 4a, the band of increased Zn content appears inside the increased Ca+P+Zn intensity band, i.e., the green band inside the white band. Note that the earlier study on Zn bands within shark centra[14] did not report Ca and P.

Figure 5a shows a synchrotron microCT slice from a block cut from the same centrum as the section in Fig. 4. The block is somewhat larger than the field of view, so only the image within the cyan dotted circle is accurate. The straight boundary at the bottom of the reconstructed solid is one of the cut surfaces. A more open structure comprises the wedge material "W" which lies to the left of the yellow dotted line segments, and the cone material "c" contains less pore volume (right side of the block). The natural surface of the cone with the intervertebral capsule, labeled "h", is the right border of the block, and has the lowest porosity. Figure 5b presents histograms of the cone material and the wedge material (within the boxes in Fig. 5a). The histograms show that the linear attenuation coefficients of the solid portions of cone and wedge are comparable, but the heights of the peaks just below 0 cm^{-1} in Fig. 5b demonstrate quantitatively that fraction of pore voxels is considerably larger within the wedge than in the cone. The differences in contrast between cone and wedge material seen in lab microCT (Fig. 3) and reported elsewhere for three carcharhiniform sharks,[7] therefore, are due to different volume fractions of porosity. A cartilage canal "cc", cut obliquely by the slices, is present in the wedge material near the cone-wedge interface. The canal diameter is about 80 µm, and the canal's axis is the radial direction of the centrum. In the lab microCT reconstruction with 18.4 µm voxels, one can barely resolve cartilage canals in the blue shark wedges.

Figure 6 enlarges a 400 x 400 x 201 voxel volume surrounding cartilage canal "cc" of Fig. 5 and shows three orthogonal sections through this volume. The transverse section (upper left of Fig. 6) is in the same orientation as the slice in Fig. 5, the three yellow arrowheads labeled "*i – iii*" indicate the positions of the sections to the right of the transverse section and the yellow arrowhead labeled "*iv*" shows the position of the orthogonal section below the transverse image. The horizontal green arrowheads indicate small 15-20 µm diameter areas enclosed by a thin layer of mineral; sometimes these appear to contain mineralized material. The side view section ("*ii*" of Fig. 6) shows that the cartilage canal "cc" runs obliquely through the volume. Side view section "*i*" demonstrates that the enclosed areas noted in the transverse section are micro-rods aligned parallel with the cartilage canal and consisting of a heavily mineralized periphery and a less mineralized interior. These micro-rods extend hundreds of micrometers.

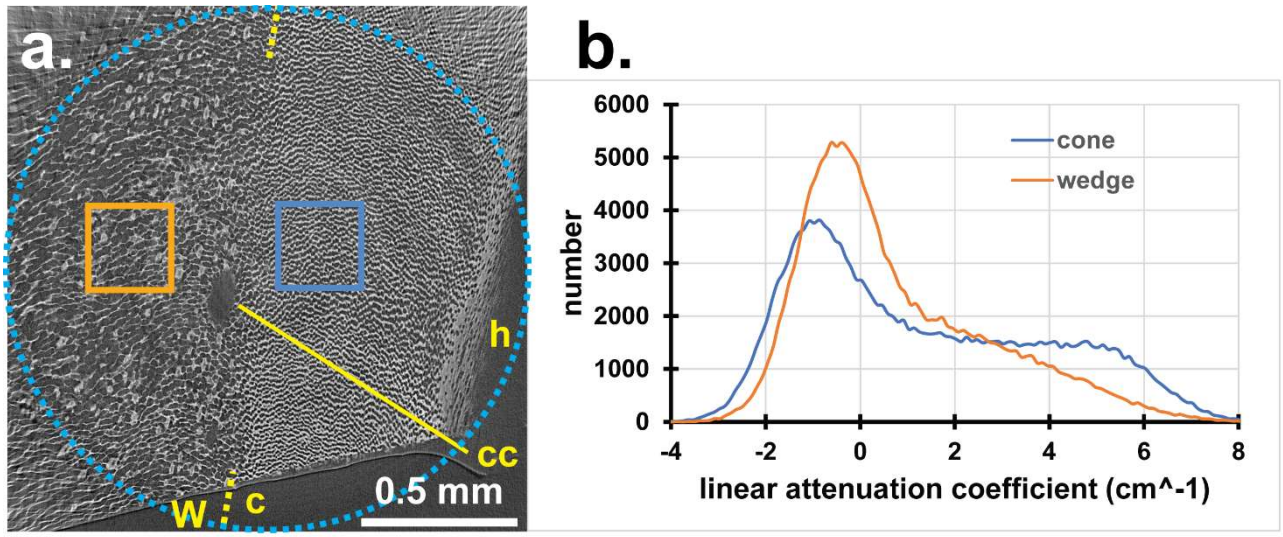

Fig. 5. (a) Synchrotron microCT slice of the blue shark centrum block with the boundary between cone "c" and wedge "W" indicated by the yellow dotted line segments. The hypermineralized portion of the cone "h", a cartilage canal "cc" and the two boxes where the histograms were measured are indicated. Reconstruction of the volume within the cyan dotted circle is with 0.69 µm voxels. (b) Histograms of 400 x 400 voxel portions of the cone (blue) and wedge (orange) materials.

Figure 7 shows the set of EDD reconstructed sections mapped with the integrated intensity of reflection q (unresolved 21.1, 11.2, 30.0 and 20.2 quadruplet of bioapatite peaks) measured with detector 5. Detector 5 measures intensity from bioapatite crystals oriented with either 21.1, 11.2, 30.0 or 20.2 lattice planes oriented to diffract in the horizontal plane, that is normal to the vertebral column axis (the centrum axial direction) and along the centrum's radial direction. Reflection q is the strongest in the EDD pattern (Fig. 8a), as expected from the reference patterns of polycrystalline hAP,[16] and this means the sections presented in Fig. 7 are the most accurate EDD map of the centrum. The cone "c" is labeled in section 1, and its inner diameter decreases until it can no longer be resolved in sections 7-11 and then increases from section 12 through 17. Part of the cone (upper boundary of Fig. 7) was not covered due to limited beam time. The wedges begin to be visible in section 3 and are no longer distinguishable in section 15 and after. By section 5 and up to section 12, the wedges and the gaps between them are easily distinguished.

In Fig. 7, very strong quadruplet intensity exists outside the centrum in the lower left corner of sections 5-7 and 12-16 (arrow pointing to section 12). Contrast of each of these two separate features is confined to a few voxels in the plane but extends through multiple sections. The contrast is also seen in precisely the same locations within EDD reconstructions with 00.2 and 13.0 diffracted intensities. Inspection of the lab microCT data set reveals small volumes of mineralized tissue within the neural arch, away from the centrum and precisely where EDD reveals diffracted intensity. Such patches normally occur within shark neural arches.[17,18] Note that almost all of the neural arch was cropped from the image shown in Fig. 1, mainly to allow the features within the centrum to be seen more clearly.

Each detector of the 6-BM-B array samples differently oriented crystallites, and comparison of different detector maps for a given reflection reveals the presence or absence of crystallographic texture. X-ray diffraction (and small angle scattering) of blocks cut from shark centra showed large azimuthal variation of 00.2 diffracted intensity, i.e., significant *c*-axis texture along well-defined anatomical directions.[6] Analogous preferred orientation of bioapatite *c*-axes exists in other collagen-based mineralized tissues including bone,[12] dentin[19] and cementum[15]. Although the individual diffraction peaks within the unresolved quadruplet reflection exhibit crystallographic texture, as can be seen in enamel,[20] the very broad diffraction 21.1, 11.2, 30.0 and 20.2 peaks (from very small crystallites) of bone, dentin and cementum produce a combined peak

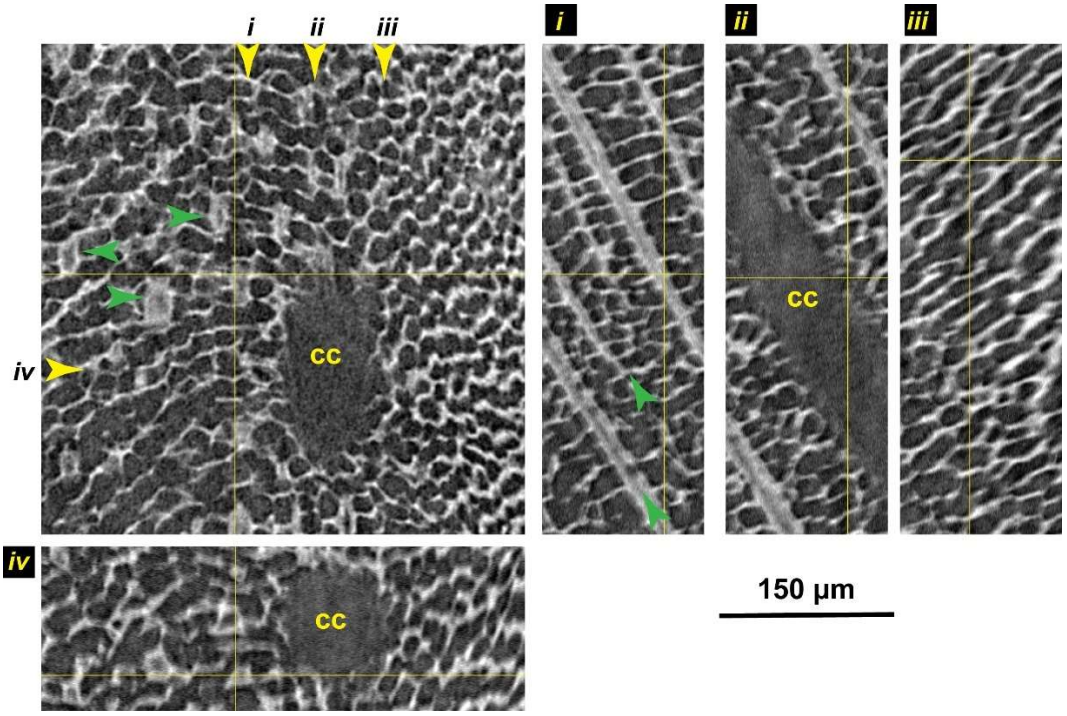

Fig. 6. Enlargement of the volume around cartilage canal "cc" in Fig. 5. The square images (upper left) is the transverse plane in the synchrotron microCT data set; the position of the orthogonal (axial) slices are indicated by the yellow arrowheads and numerals "*i–iv* ". The green arrowheads indicate the calcified micro-rods discussed in the text.

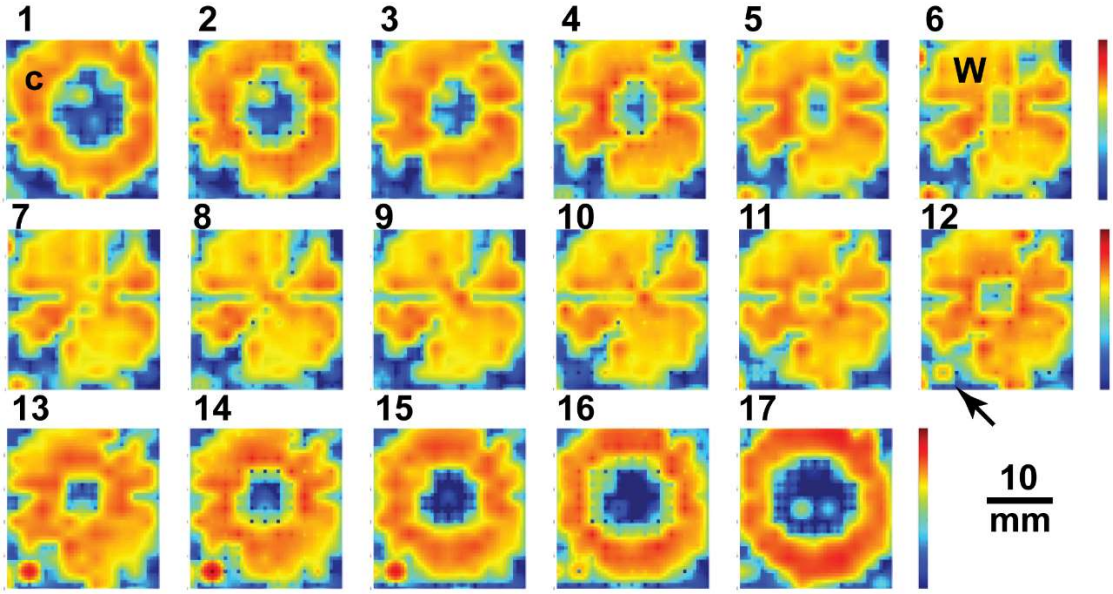

Fig. 7. Series of seventeen contiguous transverse EDD sections reconstructed with intensity from the bioapatite q reflection (unresolved 21.1, 11.2, 30.0 and 20.2 peaks). The section numbers appear above the left corner of each image. The color bars at the right of each row indicate the intensity range (log scale) which was the same for each section. The labels "c" (section 1) and "W" (section 6) identify a cone and wedge, respectively. The arrow (section 12) points to a feature discussed in the text. Ignoring rotation and allowing for the limited spatial resolution, sections 6 and 12 agree well with the lab microCT transverse section in Fig. 3. The variation of diffracted intensity within the wedges in sections 6-12 probably represents noise in the data and effects of the interpolation procedure.

does not exhibit strong texture. In addition to the relatively strong 00.2 and quadruplet peaks, Fig. 8a shows very weak but measurable 13.0 intensity in the EDD patterns from the blue shark centrum. Reconstruction with 13.0 diffracted intensity, therefore, represents a stringent test of sensitivity limits for EDD mapping. In addition, reconstruction with 13.0 intensity could provide additional texture information because the 13.0 reflection is from an *a*-*b* lattice plane and is normal to the *c*-axis.

Figure 8b compares EDD intensity maps of two sections (9 and 16) for two orthogonally-oriented detectors (1 and 5) and for two reflections (q and 13.0). Section 9 covers the wedges of the intermedialia near the centrum's axial midplane, and section 16 intersects one cone near its fullest diameter. The quadruplet maps clearly show the geometry of the structure. In section 16 of the cone, little difference exists between detector 1 and 5 maps of quadruplet intensity; and, in section 9, the quadruplet intensity maps match except for a slight difference in the bottom-most wedge intensity. For the 13.0 reflection, the detector 1 and 5 reconstructions of the cone do not appear to differ from each other nor from those of the other eight detectors (data not shown). This means that, within the cone, 13.0 does not have a preferred orientation. In the 13.0 reconstruction of section 9, however, the wedges cannot be made out in the detector 1 reconstruction but can be seen clearly in that of detector 5. Therefore, the 13.0 normals within the wedges tend to lie laterally, i.e., perpendicularly to the centrum axis, and not along the centrum's axis. Figure 9 summarizes the EDD observations of bioapatite texture.

Within the 13.0 maps of Fig. 8b, the intensity is very low, and there are "spikes" of intensity at various positions. The authors inspected each of these positions and confirmed that the automated peak fitting was problematic at these positions. This result indicates a practical limit for EDD reconstruction with weak reflections. It may be that increasing the counting time by a factor of four (and improving the signal to noise ratio by a factor of two) would help to "stabilize" the 13.0 reconstruction, but verifying this requires additional work. On balance, however, the 13.0 reflection maps of the blue shark centrum add relatively little to what is determined via the 00.2 and quadruplet maps.

As mentioned above, the quadruplet reflection's insensitivity to texture is expected. The earlier report[21] on EDD from the same blue shark centrum, showed that the bioapatite *c*-axes were aligned laterally (i.e., perpendicular to the centrum's

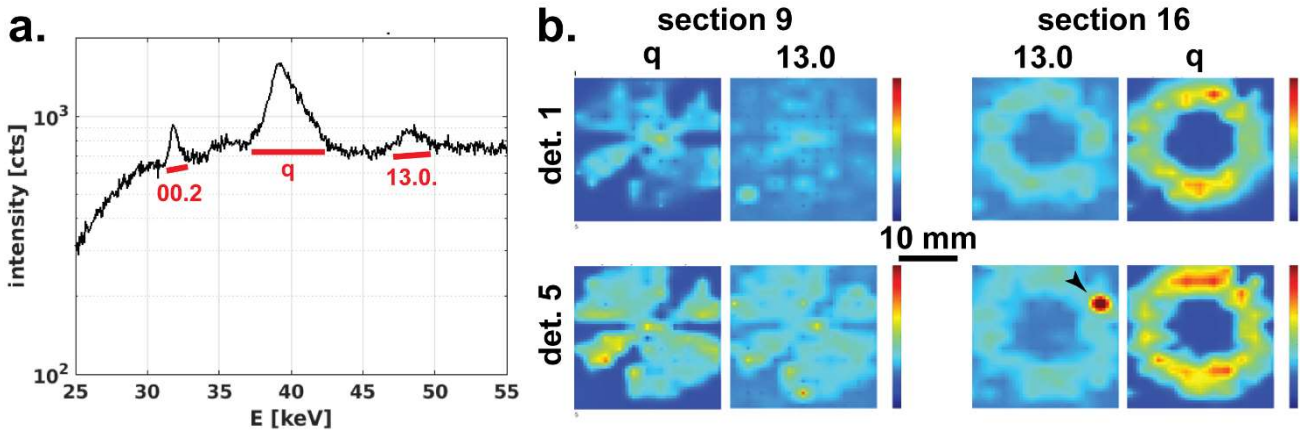

Fig. 8. (a) EDD pattern for the blue shark (sum of patterns for one Z-axis scan through the centrum). The 00.2, quadruplet "q" and 13.0 reflections are labeled. (b) Detector 1 and 5 reconstructions with the quadruplet and 13.0 intensities. Sections 9 (wedges of the intermedialia) and 16 (cone, corporus calcerea) are shown. The color bars indicate the linear intensity scale which has a minimum of -50 units and a maximum of 150 for 13.0 and of 400 for the quadruplet. The spike of intensity in the det 5, section 16, 13.0 reconstruction (black arrowhead) is discussed in the text.

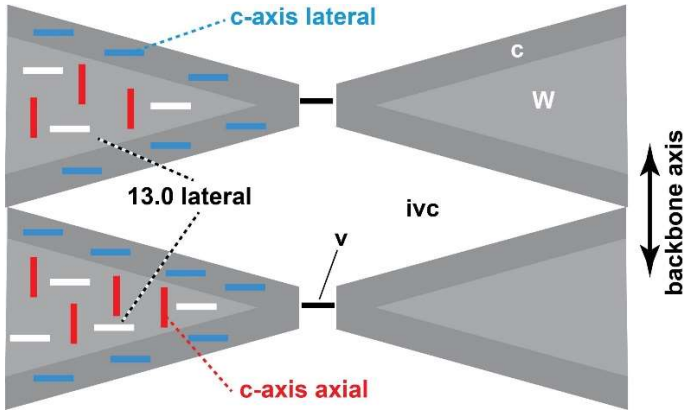

Fig. 9. Summary of crystallographic texture in the blue shark centrum observed by EDD. The red and cyan bars indicate the *c*-axis orientations determined previously.[14] The white bars indicate the 13.0 preferred orientation in the wedges (but not in the cones). c – cone, W- wedge, ivc – intervertebral capsule, v – vellum separating adjacent ivc.

axis) within the cone and axially within the wedges of the intermedialia (Fig. 9). Given that the 13.0 diffraction planes are perpendicular to the 00.2 planes, the present observation of 13.0 oriented laterally in the intermedialia is consistent with the 00.2 observation. For the cone section in Fig. 8b, little difference is seen between the two detector maps and this is surprising, at first glance, given the strong 00.2 texture. However, if the bioapatite in the cones has fiber texture (that is, only one direction is strongly oriented[13]), 13.0 has rotational freedom around the *c*-axis preferred direction, and 13.0 diffracted intensity would not vary with azimuth.

The EDD map of the blue shark centrum was one of the first obtained by the authors; as such, the experiment was aimed primarily at coverage of the entire centrum and establishing where improvements were needed. Even in this first study, the spatial variation of bioapatite texture and its relationship to anatomical structures was uncovered. Given the similarities of centra across Order Carcharhiniformes,[7] the authors predict that the lateral orientation of c-axis texture in the cones and axial c-axis texture in the wedges will be present throughout this order, something that will be proved or disproved in future studies. As discussed below, the relatively low-resolution 3D EDD maps can, when combined with much higher resolution data from absorption microCT and with elemental maps from scanning fluorescence of sections, provide substantial guidance for numerical modeling of centrum response to loading.

With the present APS bending magnet x-ray source, it is unlikely that EDD will be able to reconstruct shark centra on 3D grids smaller than 0.5 mm. Even though multiple peaks and multiple azimuths are recorded simultaneously, the relatively low diffracted intensities and long counting times are a significant constraint. With the present set-up and x-ray source, decreasing ΔX and ΔY is practical, at a cost of longer scan times or decreased volume coverage, but the sampling volume dimension along Z (δZ = 1.7 mm in the experiments described here) remains a major limitation. Oversampling along the Z-axis direction (say using ΔZ = 0.5 mm instead of ΔZ = 1.9 mm) might help overcome this limitation but scan duration would increase substantially. If higher resolution were needed in the centrum's transverse plane, one could scan the centrum using ΔZ matching the sampling volume depth (1.7 mm) as shown in Fig. 2a and then repeat the scan after rotating 90° about the Y-axis in Fig. 2a; with the long dimension of the sampling volume along two different anatomical directions, one should be able to discern sub-voxel features.

When the APS upgrade comes on-line (estimated April 2024), one expects the bending magnet flux to remain on par with the current levels and no significant improvement in measurement speed for EDD, unless a new generation detector were installed. With monochromatic x-rays from insertion devices, however, a flux increase of over two orders of magnitude is expected after the upgrade (see Fig. 2.4 of [22]). Use of sawtooth focusing-optics to define the pencil beam and conical slits[23] or spiral slits[24] to define a sampling volume, in an approach analogous to that used in the present paper, would deliver greatly increased data acquisition rates. Similar X-Y-Z translation would allow 3D reconstruction of the volume. Different azimuths would be collected simultaneously, and mapping speed would increase enormously, or, alternatively, data would be collected with much greater contrast sensitivity. Use of monochromatic high energy x-rays (E > 70 keV) would also lessen specimen dose. First, the 25-55 keV range in the present data deposits much more energy than 70+ keV photons. Second, the photons with energies between those selected for diffraction have no possibility of contributing to signal and only deposit energy in the specimen. Accumulated damage affects mechanical properties of collagen-based mineralized tissues,[25] and this could become problematic in in situ loading experiments where the same volume is observed repeatedly.

Two advantages of scanning the intact centrum with EDD is that the sampling volume is isolated from all other scattering and that all of the voxels are precisely registered with each other. Alternatively, x-ray diffraction tomography with monochromatic x-rays[26] could be used to reconstruct the texture, etc. within different sections of a block cut from a centrum like that shown in Fig. 6. Voxel sizes with monochromatic diffraction tomography could easily be on the order of 25 μm at beamline 1-ID, APS. Synchrotron microCT prescreening could identify blocks with interesting transitions and would be extremely useful in interpreting the diffraction tomography sections. Simple note-keeping suffices to locate where each block was cut from the centrum, and the simple trick of cutting the cross-section with slightly different dimensions allows orientation to be preserved. However, monochromatic diffraction tomography reconstruction as presently practiced is mathematically ill-posed; the complication of locating blocks correctly and uncertainties due to the unknown kerf thicknesses during cutting may introduce uncertainty. The EDD 3D reconstructions do not suffer from these uncertainties and provide superior sensitivity to texture.

The picture of the structure of the blue shark centrum which emerges from x-ray scattering with monochromatic x-radiation (data not presented here),[6] from synchrotron microCT, from scanning fluorescence microscopy, from lab microCT and from 3D EDD mapping is one of a hierarchy of structures spanning a wide range of spatial scales, a common theme in bioapatite mineralized tissues.[27] Taken together, the hierarchy of structures produce a shark centrum which is much more compliant than bone centra. Synchrotron microCT revealed a honeycomb of heavily mineralized material with wall thicknesses ~1-2 μm filled with soft tissue or fluid, and the difference in lab microCT contrast between cone and wedge (Fig. 3) is due to the larger proportion of unmineralized volume in the intermedialia than in the cone (Fig. 5). Earlier x-ray diffraction and small angle scattering[6] showed that the average bioapatite properties at the nanoscale (lattice parameter, crystallite size, crystallographic texture) were similar to but not identical to those of bone, a result which is not surprising given that bone is based on a type I collagen matrix and that the shark centrum matrix is cartilage (a tissue combining types I and II collagen and proteoglycans). It is unclear at this point whether the material making up the mineralized honeycomb has elastic properties similar to bone tissue or whether shark tissue is significantly less stiff at the one micrometer level. Data on 3D printed, elastomer-hAp scaffolds suggest that much of the high compliance of honeycomb-like structures during compression arises from elastic deflection of the struts and the hAp particles do not carry significant loads.[28] The observed macroscopic high compliance and large strains to failure[29] may, therefore, be due in part to the open micrometer-level structure of the centrum tissue and in part to the macroscopic architecture of the centrum.

This hypothesis, that the bioapatite-containing tissue (honeycomb walls) is not experiencing large strains but rather large displacements and rotations, can be directly tested via in situ loading and x-ray measurement of the resulting internal strains, like in the study of the 3D printed elastomer-hAp scaffold.[28] Given the dimensions of the blue shark wedges and cones, high resolution position-resolved x-ray diffraction is not required, and EDD with the 6-BM-B instrument should be able to measure such strains once a loading rig is devised. In this scheme, the bioapatite nanoparticles would function as embedded strain gages. Application of large compressions, say ~5%, and measurement of significant or insignificant internal strains would test the above hypothesis.

Within the wedges of the blue shark centrum, 15-20 μm diameter micro-rods run parallel to cartilage canals for hundreds of micrometers. Walls of the honeycomb structure link adjacent rods, and this suggests that the micro-rods serve a mechanical function. Growth bands seen in the fluorescence maps (Fig. 4) and in lab microCT (Fig. 3) scans are not readily apparent in the synchrotron microCT data sets mainly because the field of view is so small; in line with the difference in pore volume fraction observed between cone and wedge (Fig. 5), the authors speculate that the growth bands reflect small local perturbations in pore volume fraction might be quantifiable with considerable effort. Such fluctuations would they be visible in EDD maps, given their resolution. The fluorescence maps of the growth bands, in particular the intensity of Zn provides information important to understanding growth of the centra, but this is not the focus of the present discussion.

The centrum geometry measured from lab microCT could be imported into 3D models and the structural response could be calculated numerically based upon realistic boundary conditions including the presence of the fluid-filled intervertebral capsule. The EDD maps show strong crystallographic texture at the 0.5-1 mm scale, and this would require modelers to adjust elastic constants for the cone wall vs the wedge in order to capture the true response.

Additional EDD mapping of shark centra is clearly required to bolster the conclusions of this study. Perhaps finer scale maps over smaller portions of each centra would reveal nuances not noted here. Centra from additional species and from other carcharhiniform families should be mapped, with particular attention paid to 00.2 texture in the cone vs the wedges. It would also be interesting to extend the mapping to sharks of Order Lamniformes, characterized by intermedialia consisting of a set of radial lamellae instead of wedges. With such different microarchitecture and with the observation that mean mineral levels (at the 20 μm level) within cone and lamellae do not differ in lamniforms (unlike in the carcharhiniforms),[7] crystallographic texture may be absent. However, cartilage fiber orientations within cone and intermedialia, and hence bioapatite crystallographic texture, are likely basal characteristics of sharks and probably do not differ between the orders.

ACKNOWLEDGEMENTS

The lab microCT data were collected at the Duke University Shared Materials Instrumentation Facility (SMIF), a member of the North Carolina Research Triangle Nanotechnology Network (RTNN), which is supported by the National Science Foundation (Grant ECCS-1542015) as part of the National Nanotechnology Coordinated Infrastructure (NNCI); we thank Justin Gladman for his support of this imaging. Beamline 6BM-B, APS, is supported by COMPRES, the Consortium for Materials Properties Research in Earth Sciences under NSF Cooperative Agreement EAR-1661511. This research used resources of the Advanced Photon Source, a U.S. Department of Energy (DOE) Office of Science User Facility, operated for the DOE Office of Science by Argonne National Laboratory under Contract No. DE-AC02-06CH11357.

REFERENCES

[1] Porter, M.E., and Long, J.H. Jr., "Vertebrae in compression: Mechanical behavior of arches and centra in the gray smooth-hound shark (*Mustelus californicus*)," J Morphol 271, 366-375 (2010).

[2] Porter, M.E., Diaz, C., Sturm, J.J., Grotmol, S., Summers, A.P., and Long, J.H., Jr., "Built for speed: strain in the cartilaginous vertebral columns of sharks," Zool 117, 19-27 (2014).

[3] Watanabe, Y.Y., Lydersen, C., Fisk, A.T., and Kovacs, K.M., "The slowest fish: Swim speed and tail-beat frequency of Greenland sharks," J Exp Mar Biol Ecol 426/427, 5-11 (2012).

[4] Urist, M.R., "Calcium and phosphorus in the blood and skeleton of the Elasmobranchii," Endocrinol 69, 778-801 (1961).

[5] Dean, M.N., Chiou, W.-A., and Summers, A.P., "Morphology and ultrastructure of prismatic calcified cartilage," Microsc Microanal 11, 1196-1197 (2005).
[6] Park, J.-S., Almer, J.D., James, K.C., Natanson, L.J., and Stock, S.R., "Mineral in shark vertebrae studied by wide angle and by small angle x-ray scattering," J Struct Biology under review (2021).
[7] Morse, P.E., Stock, M.K., James, K.C., Natanson, L.J., and Stock, S.R., "Shark vertebral microanatomy and mineral density variation studied with laboratory microComputed Tomography," Under NOAA administrative review for submission to J Struct Biol (2021).
[8] Porter, M.E., Ewoldt, R.H., and Long, J.H. Jr., "Automatic control: the vertebral column of dogfish sharks behaves as a continuously variable transmission with smoothly shifting functions," J Exp Biol 219, 2908-2919 (2016).
[9] Kujala, N., Marathe, S., Shu, D., Shi, B., Qian, J., Maxey, E., Finney, L., Macrander, A., and Assoufid, L., "Kirkpatrick-Baez mirrors to focus hard X-rays in two dimensions as fabricated, tested and installed at the Advanced Photon Source Source," J Synchrotron Rad 21, 662 - 668 (2014).
[10] Brister, E.Y., Vasi, Z., Antipova, O., Robinson, A., Tan, X., Agarwal, A., Stock, S.R., Carriero, A., Richter, C.-P., "'X-ray fluorescence microscopy: A method of measuring ion concentrations in the ear," Hearing Res 391, 107948 (2020).
[11] Weidner, D.J., Vaughan, M.T., Wang, L., Long, H., Li, L., Dixon, N.A., and Durham, W.B., "Precise stress measurements with white synchrotron x-rays," Rev Sci Instrum 81, 013903 (2010).
[12] Almer, J.D., and Stock, S.R., "Internal strains and stresses measured in cortical bone via high-energy x-ray diffraction," J Struct Biol 152, 14-27 (2005).
[13] Cullity, B.D., and Stock, S.R. [Elements of X-ray Diffraction], 3rd Ed., Prentice-Hall: Upper Saddle River (2001).
[14] Raoult, V., Howell, N., Zahra, D., Peddemors, V.M., Howard, D.L., de Jonge, M.D., Buchan, B.L., and Williamson, J.E., "Localized zinc distribution in shark vertebrae suggests differential deposition during ontogeny and across vertebral structures," PLoS One 13, e0190927 (2018).
[15] Stock, S.R., Finney, L.A., Telser, A., Maxey, E., Vogt, S., and Okasinski, J.S., "Cementum structure in Beluga whale teeth," Acta Biomater 48, 289-299 (2017).
[16] Powder Diffraction File 00-86-2101, International Centre for Diffraction Data.
[17] Bordat, C., "Etude ultrastructurale de l'os des vertebres du Selacien *Scyliorhinus canicula* L.," Can J Zool 65, 1435-1444 (1987).
[18] Dean, M.N., and Summers, A.P., "Mineralized cartilage in the skeleton of chondrichthyan fishes," Zool 109, 164-168 (2006).
[19] Almer, J.D., and Stock, S.R., "Loading-related strain gradients spanning the mature bovine dentinoenamel junction (DEJ): Quantification using high energy x-ray scattering," J Biomech 43, 2294-2300 (2010).
[20] Free, R., DeRocher, K.D., Xu, R., Joester, D., and Stock, S.R., "A method for mapping submicron-scale crystallographic order/disorder applied to human tooth enamel," Powder Diffraction 35, 117-123 (2020).
[21] Park, J.-S., Chen, H., James, K.C., Natanson, L.J., and Stock, S.R., "Three-dimensional mapping of mineral in intact shark centra with energy dispersive x-ray diffraction," J Mech Behav Biomed Mater under review (2021).
[22] Stock, S.R. [MicroComputed Tomography: Methodology and Applications], 2nd Ed., Taylor and Francis: Boca Raton (FL) (2019).
[23] Park, J.S., Lienert, U., Dawson, P.R., and Miller, M.P., "Quantifying Three-Dimensional Residual Stress Distributions Using Spatially-Resolved Diffraction Measurements and Finite Element Based Data Reduction," Exp Mech 53, 1491–1507 (2013).
[24] Martins, R.V., Ohms, C., and Decroos, K., "Full 3D spatially resolved mapping of residual strain in a 316L austenitic stainless steel weld specimen," Mater Sci Eng A 527, 4779–4787 (2010).
[25] Barth, H.D., Zimmermann, E.A., Schaible, E., Tang, S.Y., Alliston, T., Ritchie, R.O., "Characterization of the effects of x-ray irradiation on the hierarchical structure and mechanical properties of human cortical bone." Biomater 32, 8892-8904 (2011).
[26] Gursoy, D., Bicer, T., Almer, J.D., Kettimuthu, R., De Carlo, F., and Stock, S.R., "Maximum a posteriori estimation of crystallographic phases in X-ray diffraction tomography," Phil Trans Roy Soc (Lond) A 373, 20140392 (2015).
[27] Lowenstam, H.A., and Weiner, S., [On Biomineralization], Oxforld Univ. Press: Oxford (1989).
[28] Stock, S.R., Park, J.-S., Jakus, A., Birkbak, M., Frølich, S., Birkedal, H., Shah, R., and Almer, J.D., "*In situ* loading and x-ray diffraction quantification of strains in hydroxyapatite particles within a 3D printed scaffold," Materialia 18, 101174 (2021).
[29] Ingle, D.I., Natanson, L.J., and Porter, M.E., "Mechanical behavior of shark vertebral centra at biologically relevant strains," J Exp Biol 221, 188318 (2018).